Journal of Neuroscience Methods 204 (2012) 355–365

Contents lists available at SciVerse ScienceDirect

Journal of Neuroscience Methods

journal homepage: www.elsevier.com/locate/jneumeth

Basic Neuroscience

Insect-machine interface: A carbon nanotube-enhanced flexible neural probe

W.M. Tsang[a], Alice L. Stone[b], David Otten[a], Zane N. Aldworth[c], Tom L. Daniel[c], John G. Hildebrand[b], Richard B. Levine[b], Joel Voldman[a,*]

[a] Electrical Engineering and Computer Science, Massachusetts Institute of Technology, USA
[b] Department of Neuroscience, University of Arizona, USA
[c] Department of Biology, University of Washington, USA

ARTICLE INFO

Article history:
Received 10 August 2011
Received in revised form
19 November 2011
Accepted 21 November 2011

Keywords:
Moth
Neural probe
Carbon nanotube
Microfabrication
Wireless system

ABSTRACT

We developed microfabricated flexible neural probes (FNPs) to provide a bi-directional electrical link to the moth *Manduca sexta*. These FNPs can deliver electrical stimuli to, and capture neural activity from, the insect's central nervous system. They are comprised of two layers of polyimide with gold sandwiched in between in a split-ring geometry that incorporates the bi-cylindrical anatomical structure of the insect's ventral nerve cord. The FNPs provide consistent left and right abdominal stimulation both across animals and within an individual animal. The features of the stimulation (direction, threshold charge) are aligned with anatomical features of the moth. We also have used these FNPs to record neuronal activity in the ventral nerve cord of the moth. Finally, by integrating carbon nanotube (CNT)-Au nanocomposites into the FNPs we have reduced the interfacial impedance between the probe and the neural tissue, thus reducing the magnitude of stimulation voltage. This in turn allows use of the FNPs with a wireless stimulator, enabling stimulation and flight biasing of freely flying moths. Together, these FNPs present a potent new platform for manipulating and measuring the neural circuitry of insects, and for other nerves in humans and other animals with similar dimensions as the ventral nerve cord of the moth.

1. Introduction

The development of insect-machine interfaces (IMIs) is beneficial to both biologists and engineers. Traditionally, IMIs provide tools for biologists to study the neural circuitry of insects, which present tractable models of neurobiological systems (Burrows, 1996). Alternatively, there has been an increasing interest in combining living insects with microsystems to form "biobots" with functionality beyond that possible from purely synthetic robots. For both of these applications, the ideal IMI should be able to provide a robust and reliable communication link between the insect and the machine. Thus, the IMI should be able to deliver stimuli from the machine to the insect, as well as to capture neuronal signals from the insect to the machine. However, the small size of insects presents a challenge for most existing technologies, which typically focus on applications for large animals such as mammals.

Classically, insulated (except at the tip) thin metal wires or hand-made clip electrodes are employed for IMIs. For examples, researchers have employed clip electrodes and tungsten wire to record neural activity from the ventral nerve cord (VNC), which carries axons between ganglia of the central nervous system (CNS), of tethered cockroaches (Ye et al., 1995) and freely behaving locusts (Harrison et al., 2010) to study their escape behavior. Alternatively, engineers have attempted to create insect-based micro-air-vehicles (i-MAVs) by implanting metal wires into the brain and wing muscles of beetles (Sato et al., 2009) and moths (Bozkurt et al., 2009; Daly et al., 2010) and using electrical stimulation to bias their flight path. Although promising results have been achieved using these electrodes, the number of stimulation (or recording) sites, production efficiency, and reproducibility of these electrodes are intrinsically limited due to the manual nature of their production. Advances in microfabrication, however, create the possibility to develop robust multi-site neural probes for small animal systems. Three-dimensional shape-memory alloy microelectrodes (Takeuchi and Shimoyama, 2000) and silicon- or polymer-based flexible insertion microelectrodes (Gray et al., 2002; Lemmerhirt et al., 2006; Spence et al., 2007) have been applied for IMIs, albeit only for neuronal recording.

Recently, we reported a microfabricated flexible neural probe (FNP) that contains a polyimide-gold-polyimide split-ring structure to interface with the VNC of the moth *Manduca sexta* and to allow an efficient probe implantation process as shown in Fig. 1 (Tsang et al., 2010). The FNP can stimulate multi-directional graded abdominal motion in both pupae and adult moths. Moreover, in loosely tethered flight, we have used stimulation through the FNP to bias the flight path of moths. However, the FNP requires a relatively high

* Corresponding author. Tel.: +1 617 599 2094.
E-mail address: voldman@mit.edu (J. Voldman).

0165-0270/$ – see front matter © 2011 Elsevier B.V. All rights reserved.
doi:10.1016/j.jneumeth.2011.11.026

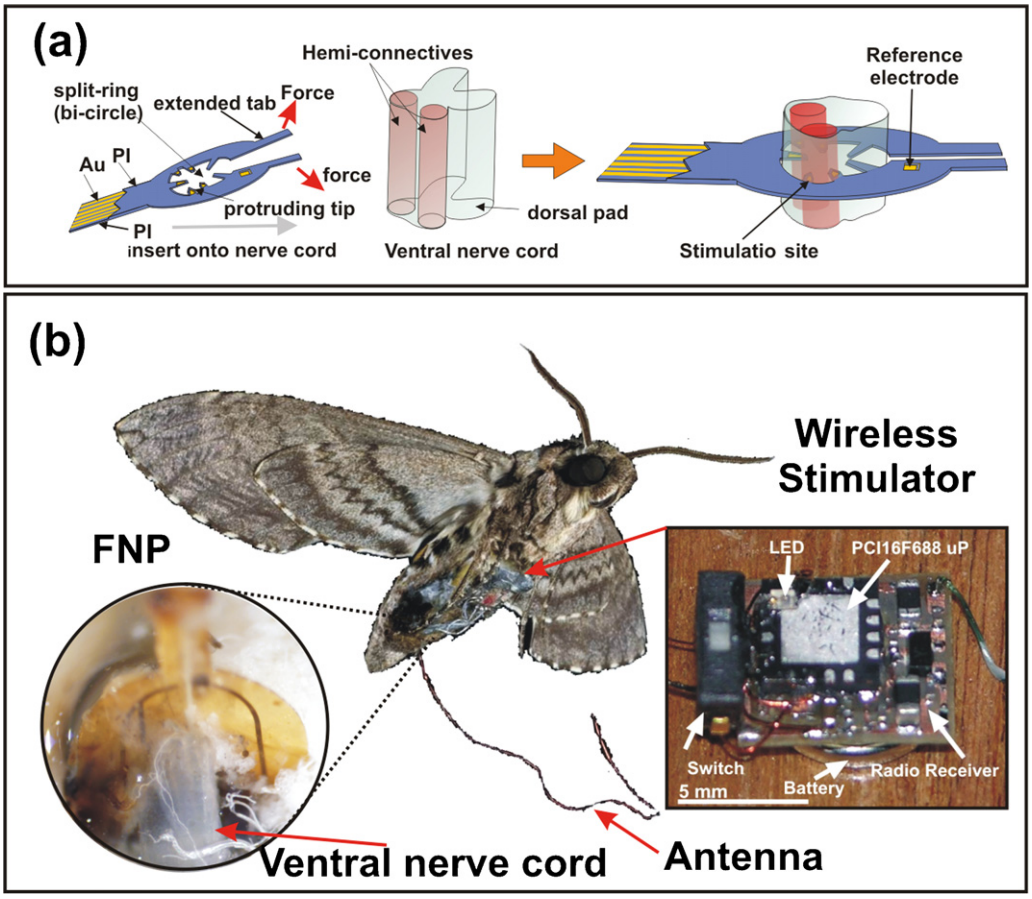

Fig. 1. i-MAVs and FNP implantation. (a) Schematic of the FNP insertion process, showing how the split-ring can be opened to fit around the VNC. (b) Illustration of i-MAV including moth, FNP and wireless stimulator.

stimulation voltage (5–10 V) to evoke a sufficiently strong abdominal motion to bias flight. This stimulation voltage is higher than the typical output (≤4.0 V) of most compact wireless stimulators (Bozkurt et al., 2009; Daly et al., 2010; Sato et al., 2009). Furthermore, although FNP stimulations induce repeatable motions in a single animal, the motions are inconsistent across animals, and <50% of moths exhibited both left and right abdominal motions in response to FNP stimulation. For reliable biasing of flight, it is important to develop a microfabricated FNP that can elicit the same abdominal response from any moth (e.g. right or left movement) with a given set of stimulation parameters. In addition, with appropriate stimulation parameters, it must be possible to evoke both left and right abdominal movements from nearly every moth.

In this work, we developed an improved FNP with significantly enhanced performance and new capabilities. To lower stimulation voltage, we developed an electroplating method to integrate carbon nanotube (CNT)-Au nanocomposites onto the FNP to enhance its charge-injection capability, which allows the stimulation voltage of the FNP to be compatible with typical wireless stimulators. To improve repeatability, we re-designed the geometry of the FNP to match more nearly the anatomical structure of the insect's VNC, toward the goal of achieving more consistent abdominal responses. The new design contains five stimulation sites (area: 900–1300 μm^2) inside a bi-cylinder split-ring structure to match the bi-cylindrical structure of the moth's VNC and a large stimulation site (14,400 μm^2) outside of the split ring region to act as reference electrode as schematically shown in Fig. 1a. To quantify the performance of the FNP, we developed a custom stimulation and measurement system that allows computer-controlled stimulation and automated image analysis of the resulting abdominal motion. Moreover, we demonstrated the ability of CNT-Au-coated FNPs (C-FNPs) to record neuronal signals from the VNC of the moth, establishing the ability both to stimulate and to record from insects using the FNP. Finally, we integrated the C-FNPs with a wireless system to remotely alter the flight path of moth and thus to demonstrate the possibility for creating i-MAVs (Fig. 1).

2. Materials and methods

2.1. Probe fabrication and packaging

The FNP is made of two layers of polyimide (PI) with gold sandwiched in-between in a split-ring geometry (Fig. 1a). The main steps of FNP fabrication (Fig. 2) are similar to those previously reported (Tsang et al., 2010). The CNT-Au nanocomposite coating is applied from an aqueous solution (1 mg/mL) consisting of multi-wall CNTs (Cheap Tubes Inc.) mixed into a Au-electrolyte bath (TSG-250, Transene) with monophasic voltage pulses (1.0 V, 50% duty cycle, 1.5 min). The CNTs have a length of 0.5–2.0 μm and a diameter <8 nm.

To package the probes, we connected them to cables using FFC\FPC connectors (FH19SC-6S-0.5SH, Hirose Electric Co. Ltd.), or 50-μm teflon-coated stainless steel wires (790600, A-M Systems)/teflon-coated Ag wires (785500, A-M Systems) with conductive epoxy (CW2400, ITW Chemtronics). The connecting regions are further sealed with insulating epoxy (Scotch-weld 2216 B/A, 3 M), to enhance the mechanical attachment between the electrode and wires.

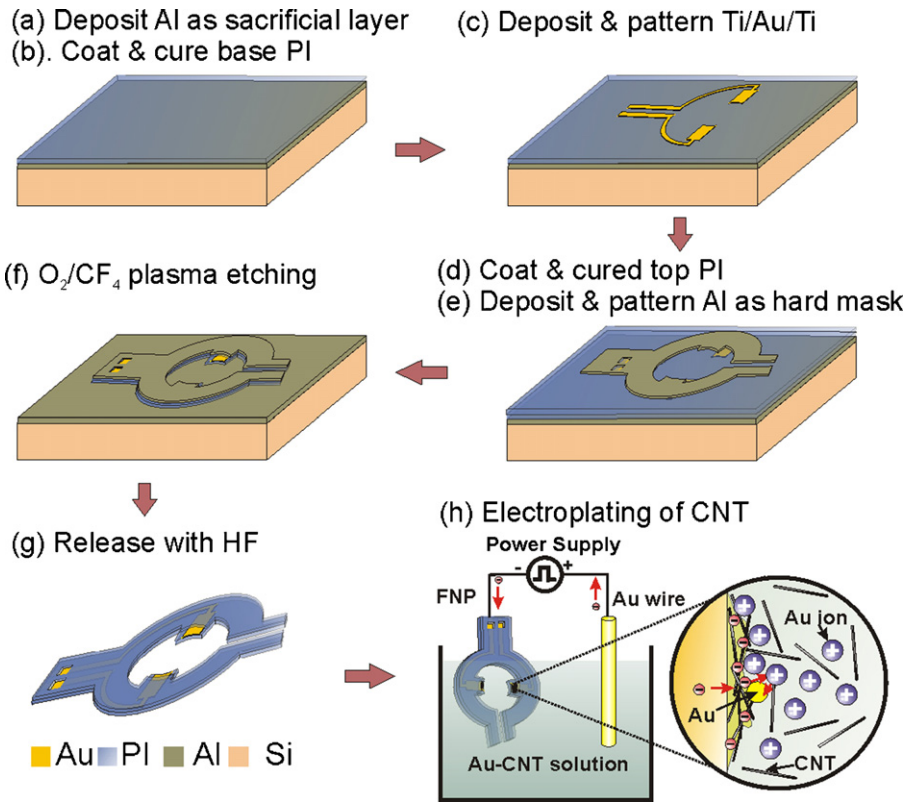

Fig. 2. The fabrication process of C-FNPs. (a) Deposit Al as sacrificial layer; (b) coat and cure base PI layer; (c) deposit and pattern Ti/Au/Ti layer as the electrical conductive traces; (d) coat and cure top PI layer; (e) deposit and pattern Al layer as hard mask for dry etching; (f) pattern the FNP structure by O_2/CF_4 plasma etching; (g) release the FNP from the substrate by dissolving the sacrificial Al layer in HF; (h) coat CNT-Au nanocomposites onto FNP by electroplating.

2.2. *In vitro characterization of probes*

The charge transport properties of the FNP were studied by electrochemical impedance spectroscopy (EIS) in 1× phosphate buffered saline (PBS). The measurements were performed via a potentiostat (VersaSTAT3, Princeton Applied Research) with a micro-cell kit (Model K0264, Princeton Applied Research). The EIS measurements were performed using a two-electrode configuration with a Pt wire as the counter electrode. The measurements were taken between 1 Hz and 100 kHz using a 10 mV ac signal and used to fit with an equivalent circuit model using Zview (Scribner Associates, Inc.).

2.3. *Probe implantation*

Mature male pupae of the moth *Manduca sexta* eclosed in wax-lined bags kept in an environmental chamber (Percival) at 29 °C, RH ~80%, and continuous light (27 lum/sf). FNPs were implanted in adult male moths on the first day of post-eclosion, after the wings were fully inflated and hardened. Animals were anesthetized by chilling under ice for 1–4 h. As shown in Fig. 3, scales were vacuum aspirated from ventral abdominal segments 1–3, from the tip of the abdomen, and from the dorsal thorax. The exposed cuticle of the abdomen tip and dorsal thorax was scratched with sandpaper to improve glue adhesion. Moths were placed ventral side up in a glass dish surrounded by ice, and damp Kimwipes (Fisher Scientific) were used to secure the moth's legs away from the surgical field (Fig. 3a). A horizontal incision was made in the center of the ventral surface of the 3rd abdominal segment and joined via a short lateral vertical cut to another horizontal incision near the posterior edge of the segment (Fig. 3b). This "trapdoor" incision was folded to the left and secured with a damp Kimwipe. A blunt glass probe was used to isolate the VNC, and a sharpened glass probe was used to create a small hole penetrating the sheath of the VNC into the connective tissue between the two (axon-bearing) hemiconnectives (Fig. 3c). The FNP was manipulated onto the VNC so that the extended tabs separated and the connective slid between them and into the split ring (Fig. 3d). The stimulation site at the base (site 3) of the split-ring was pushed into the prepared hole to secure the FNP in a stable position (Fig. 3e). Small pieces of Gelfoam® (absorbable gelatin sponge, Pharmacia) were added to each side of the FNP and tucked into the body. The depth markings on the FNP were aligned with the incision closure as the flap of cuticle was returned to its native position, leaving a large portion of the FNP extending outside the body (Fig. 3f). The incision was closed using 3 M Vetbond glue (Animart) with an outer layer of Loctite 4013 adhesive (RS Hughes) (Fig. 3g). While this glue polymerized, a small red dot (3 mm diameter) was glued to the tip of the abdomen using a drop of Loctite 4013. Saline was dripped over the area to speed polymerization. The moth was removed from the dish and turned over, and a moistened cardboard tab was affixed to the dorsal thorax using Loctite 4013. This tab served as a handle for tethering the moth during experiments and also secured the wires extending from the FNP to decrease the chance that a tug on the wires could dislodge the implant. Moths with implanted FNPs were returned to wax-lined bags, housed in the same environment described above, and allowed to recover overnight prior to stimulation or neural recording experiments.

2.4. *Tethered stimulation*

A custom multi-channel stimulator capable of either current-controlled or voltage-controlled operation was used to generate stimuli and to measure the corresponding voltage/current data.

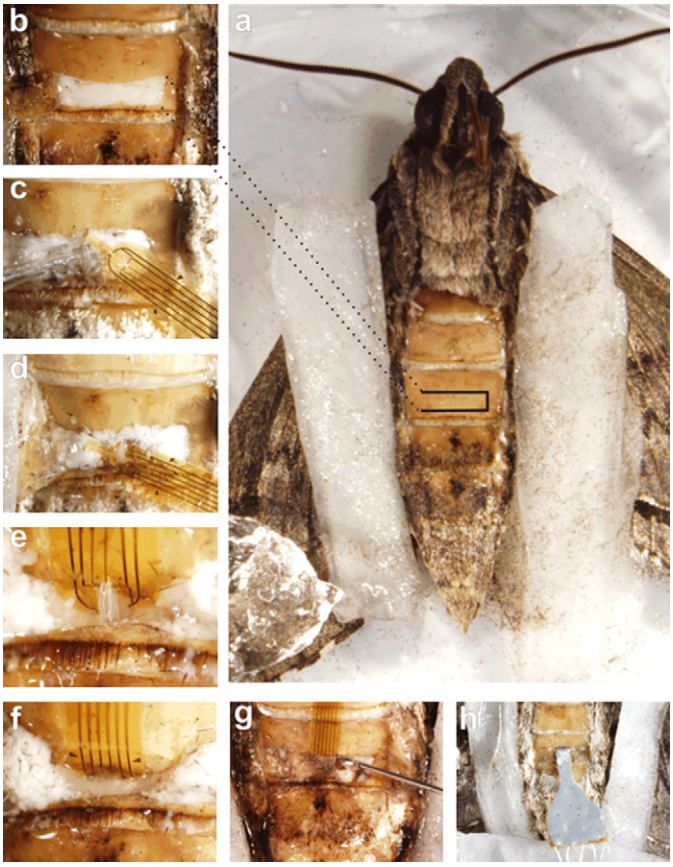

Fig. 3. Implantation of FNP into adult moth. (a) Anesthetize moth, ventral side up, box shows incision site; (b) create trap-door incision at base of third abdominal segment; (c) isolate the VNC on glass probe, place FNP nearby; (d) open FNP and bring it onto the VNC, with site 3 penetrating into the connective tissue between the axon-bearing hemiconnectives; (e) position FNP for insertion into the body, VNC is visible passing through split ring; (f) insert FNP so that the VNC lays at its natural depth, align marks with incision edge, add Gelfoam to both sides of FNP; (g) reposition trapdoor piece of cuticle and glue in place; (h) shows actual implanted FNP at conclusion of surgery, animal can be stimulated the next day.

Abdominal responses of an implant-bearing tethered moth were recorded by a webcam (LIVE! CAM Optia AF, Creative) at a frame rate of 15 frames per second and a resolution of 640 × 480 pixels. Both the stimulator and webcam were controlled by a MATLAB script through the computer's USB port. The responses of a moth were characterized by tracking the location of the red dot (3 mm in diameter) that had been applied to the tip of the moth's abdomen (Fig. 4a).

Fig. 4b shows a block diagram of the stimulator. The operation of the device started with parameters entered into the microprocessor (PIC 18F8722, Microchip Inc.) from a computer using the serial interface or manually using the LCD display (Fig. 4c) and 4 push-button switches. The microprocessor generated the required waveform with a 16-bit D/A converter. This was converted to a current signal with the current source or buffered with the voltage source. A 2:1 multiplexer selected the voltage or current signal. A 16:1 multiplexer connected the signal to the required electrode. A second 16:1 multiplexer was used to connect one of the other electrodes to ground. Both the current and voltage of the synthesized waveform were measured with sensors. These signals were available on BNC connectors and could be viewed on an external oscilloscope. They were also digitized with two 16-bit A/D converters and the data stored in memory on the microprocessor for later downloading to a computer with the serial interface.

The most difficult function of the signal source to implement was the current source. High-voltage (±10 V), precise (1%), bidirectional current sources are not available as integrated circuits. Operational amplifiers can be configured to simulate a current source, but their performance depends on the load, which is largely unknown in this application. Transistors have inherent current source behavior but are not well controlled over temperature. The circuit shown in Fig. 4d takes a bipolar voltage signal and converts it to a bidirectional current signal. Operational amplifiers U15A and B convert the voltage signal to a current through Q9 and Q10. This current is then replicated with two 4-transistor current mirrors. Q1–Q4 are used for positive currents and Q5–Q8 are used for negative currents.

We used biphasic voltage pulses, with a waveform (2 ms duration, 100 pulses at a repetition rate of 200 pulses per second) identical to that reported previously (Tsang et al., 2010) for the CNT-Au nanocomposite characterization (Fig. 4e). We used charge-balanced biphasic current pulses to characterize the stimuli (Fig. 4e). The current pulses had a slightly different shape from the voltage pulses (3 ms duration), but the same pulse number and repetition rate.

2.5. Wireless stimulation

The wireless stimulator (Fig. 1b, inset) was assembled from commercially available components and powered by a rechargeable battery (ML612S, Panasonic). The system had a single-channel AM receiver (microflierradio) to receive signals (27 MHz) from the transmitter and a microcontroller (PIC16F688, Microchip Technology) to generate biphasic voltage pulses for the stimulations (6 channels). The dimensions and the mass of the system were 6.8 mm × 10.2 mm × 5.1 mm and ~460 mg, respectively, which was small enough to be carried by all moths tested ($n > 10$). The operating range and time of the system were ~3 m and ~30 min, respectively, starting with a fully charged battery. The magnitude of the pulse was equal to the voltage of the battery (≤2.5 V), and the frequency and duration of the stimulation signal were controlled via the transmitter. For the wireless experiments in this paper, the duration of the frequency and the duration of the stimulation signal were fixed to 200 Hz and 1 ms, respectively. In total, 100 pulses were applied for each stimulation.

2.6. Neuronal recording

Neuronal signals from the moth's VNC were captured by the CNT-Au nanocomposite-coated FNPs. The differential signal from two stimulation sites of the probe was amplified (1000×, A-M Systems Model 1700) before being sent to a data acquisition system (Axon CNS, Digidata 1440A). The signal was then sampled at 10 kHz and recorded and stored in a computer using commercial software (Clampex 10.2). Spike sorting was accomplished using Wave_clus software (Quiroga et al., 2004).

3. Results and discussion

3.1. Improved FNP design

We re-designed the FNPs to improve their performance electrically and biologically. The essential FNP design, which allows the user to open the split-ring of the FNP during insertion around the VNC (Fig. 1a), remains unchanged. Two extended tabs at the tip of the FNP act as "handles" to manipulate the implant and lock the FNP in place after the insertion. However, the improved FNP design (Fig. 5) better accommodates the bi-cylindrical anatomy of the VNC (Fig. 1a, Fig. 5d–e), as opposed to the prior FNP design that was best-suited for a single cylindrical nerve cord structure. Additionally, the improved FNP has an additional stimulation site outside

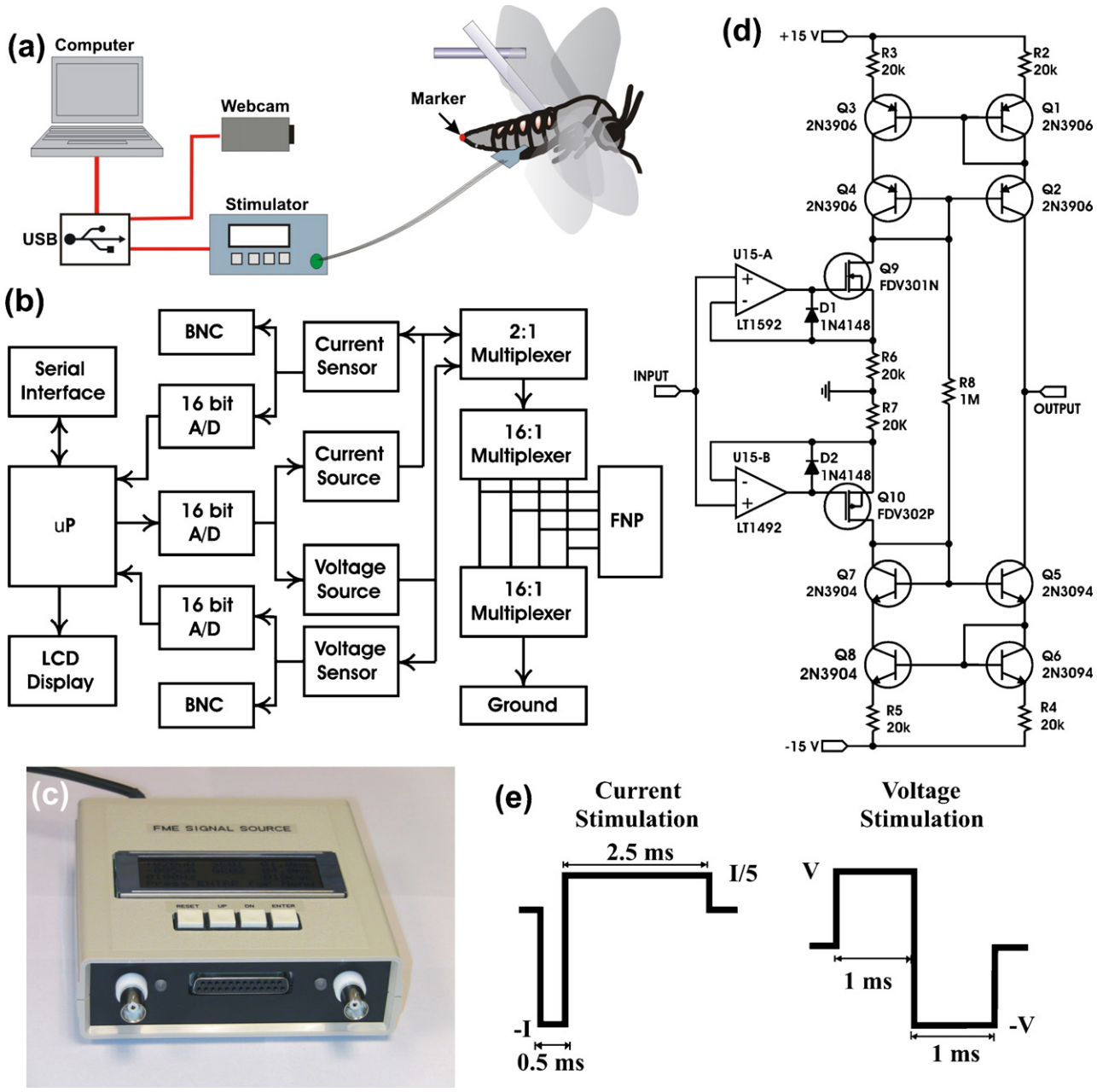

Fig. 4. Tethered stimulation system. (a) Schematic of the tethered stimulation system. (b) Block diagram of the multi-channel stimulator. (c) Image of finished stimulator. (d) Schematic of current source circuit. (e) Waveforms of the stimulation signals.

of the split ring region to act as a reference electrode (Fig. 5b). Hence, the improved FNP design allows us to excite axons within the VNC under a specific stimulation site through a stimulation site pair containing the reference electrode and that stimulation site. In contrast, for the prior FNP design all stimulation sites were located inside the split-ring, therefore, it would simultaneously excite axons within the VNC under both stimulation sites of the stimulation pair reducing the selectivity for the FNP stimulation. Hence, fewer than 50% of moths in our previous experiment exhibited both left and right abdominal motions in response to FNP stimulation.

Additionally, because all the stimulation sites in the prior FNP design are uniformity distributed in the circular split-ring structure, a significant variation in the orientation of stimulation sites relative to the VNC can result from different preparations or movement after implantation, leading to inconsistent stimulation response among the animals. Hence, for the improved FNP design, one of the stimulation sites (site 3) at the base of the split-ring was designed to penetrate into the connective tissue between the axon-bearing hemiconnectives, anchoring the probe in a consistent position (Fig. 5d). Finally, we added holding tips at the top of the split-ring (Fig. 5b), which insert into the dorsal pad of the nerve cord (non-neural tissue, Fig. 5d) to support the probe physically and prevent it from moving. These holding tips do not contain any stimulation sites as there are no neuronal processes in the dorsal pad. All of the axons within the VNC are located in the hemi-connectives as shown in Fig. 5e. We implanted the improved FNP into 29 adult moths. All of the animals remained alive more than 2 days (some up to 6 days) after the probe implantation and were extensively stimulated (>200 times) each day. Moreover, we did not observe any unusual behaviors in these animals that would indicate damage to the VNC attributable to the FNP implantation.

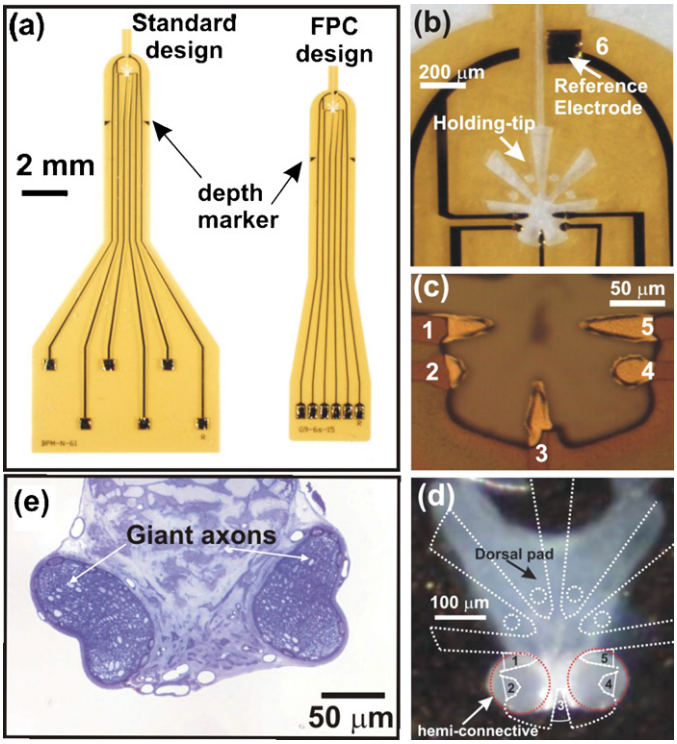

Fig. 5. Design of FNPs and anatomical structure of moth's VNC. (a) Image showing the dimensions of various FNP designs. The standard design uses epoxy connections while the FPC design is matched to flexible printed circuit board connectors. Close-up images of (b) the head showing the location of site 6 reference electrode and holding-tips and (c) the split-ring structure showing the bi-circle design of the FNP. (site areas; 1, 5: 1460 μm^2; 2, 4: 900 μm^2, 3: 1300 μm^2 and 6: 14,400 μm^2). (d) Image of a cross section of the VNC of the adult moth overlaid with scaled schematized drawings of the split-ring of the FNP. (e) Histological section of the hemi-connectives showing the distribution of the giant axons.

3.2. CNT-Au nanocomposites

In addition to geometrical improvements in the FNP, we wanted to improve the electrical performance, namely to improve the interfacial impedance in order to decrease the stimulation voltage and allow the ability to record. Various high charge-injection capability materials, including platinum black and iridium oxide, have been coated onto neural probes to improve the interfacial impedance, but their physical and chemical stability are challenging. Alternatively, carbon nanotubes (CNT) have a high charge-injection capability while also showing excellent chemical and physical stability (Voge and Stegemann, 2011). Furthermore, purified CNTs have been demonstrated to be a good growth surface for neurons and to promote an increase in the efficacy of neural signal transmission, indicating their biocompatibility (Lovat et al., 2005). In this work, to improve interfacial properties, we adapted a CNT-Au nanocomposite coating that modified from previously reported method (Keefer et al., 2008) for use with the FNP. After coating the substrate with the CNT-Au nanocomposite, we observed that nano-protrusions developed on the surface of the stimulation sites (Fig. 6a–b).

Electrical measurements of representative FNP and CNT-Au-nanocomposite-coated FNP (C-FNP) in saline solution using EIS are shown in Fig. 6c along with a standard equivalent-circuit model for the probe. In the model, the interface between the probe and saline is represented by a constant phase element (CPE, with impedance $Z_{dl} = 1/C_{dl}(j\omega)^n$, for an ideal capacitor $n = 1$) in parallel with the Faradaic impedance R_f, while R_s is the spreading resistance of the solution. The charge injection capability of the probe is proportional to the value of C_{dl}. The extracted values of C_{dl} increase from 1.84×10^{-9} F s^{n-1} (i.e. 66 μF s^{n-1}/cm^2) to 51×10^{-9} F s^{n-1} (i.e. 1.8 mF s^{n-1}/cm^2) (Fig. 6d) following the coating and are comparable to the reported values for other popular coating materials such as iridium oxide (2.1 mF s^{n-1}/cm^2) and platinum black (6.6 mF s^{n-1}/cm^2) (Malleo et al., 2010). The extracted value of n increases from 0.88 to 0.94 following the coating (not shown). Additionally, the interfacial impedance at the biologically relevant frequency of 1 kHz decreases from 408 kΩ to 13.8 kΩ (Fig. 6e) following the coating, demonstrating that the interfacial properties of the probes are significantly improved ($p < 0.001$, $N = 50$ stimulation sites), which we attribute to the formation of the nano-protrusions. Finally, *in vivo* characterization shows that the C-FNPs are able to elicit abdominal motion of the moths with a stimulation voltage significantly less (1.0 V vs. 2.0 V, $p < 0.001$, $N = 10$ moths) than that of uncoated FNPs. Thus, the CNT-Au nanocomposite substantially improves the interfacial properties of the FNPs. Furthermore, we did not observe any differences, in term of the life-cycle and behaviors, between animals implanted with FNP and C-FNP.

3.3. Electrical stimulation

One of the primary improvements in the FNP was the geometrical change to better accommodate the anatomy of the VNC. To evaluate whether the geometrical changes improved performance, we developed an experimental setup capable of quantitatively measuring moth abdominal motion in response to stimulation (Fig. 4a). Using this system, we delivered electrical stimuli into the VNC of the moth by injecting biphasic current pulses through a pair of stimulation sites on the probe. We used biphasic current pulses to minimize tissue damage and electrode corrosion (He, 2005; Merrill et al., 2005; Peckham and Knutson, 2005). Additionally, with the current-controlled stimulation, the quantity of charge delivered per stimulus pulse is not affected by the changes in the tissue load. In our current pulses, the first phase (cathodic) of the pulses was used to excite axons in the VNC and the second phase (anodic pulse) of the pulses was used to reverse the direction of electrochemical processes occurring during the first phase (Fig. 4e). The absolute magnitude of the second phase was five times lower than that of the first phase to reduce the suppressing effect of the second phase on neuronal excitation (He, 2005; Merrill et al., 2005; Peckham and Knutson, 2005) but the pulse width of the second phase (2.5 ms) was five times longer than that of the first phase (0.5 ms) to maintain the charge balance.

Representative stimulation results are shown in Fig. 7. We measured the magnitude (r) and direction (θ) of the abdominal movement by the position of the red dot on the abdominal tip of the moths. We found, not unexpectedly, that the abdominal motion of the moth increased with the magnitude of the stimulation signal, from no discernable motion at 1.25 μA to 5.7 mm displacement at 5 μA and 6.7 mm displacement at 10 μA (Fig. 7a). The evoked abdominal motions were generally repeatable for successive stimulations (≥10) as shown in Fig. 7b, with a standard deviation of 7.9% for r and 2.3% for θ. On the other hand, the direction of the evoked abdominal motions was consistent and the electrical impedance of the FNP-neural interface was stable for the entire lifetime (up to 6 days) of the post-implanted moths as shown in Supplementary Fig. S1.

Additionally, we measured the voltage across pairs of stimulation sites during current pulse delivery (Fig. 7c), and, we thus could estimate the power consumption for stimulation from the product of the stimulation voltage and current. The charge conduction between the probe and neural tissue (i.e. electrolyte) is attributed to capacitive charging in the electron double layer at the neural-probe interface and the Faradaic reaction of chemical species in the electrolyte. Upon delivery of current in the first cathodic pulse, the

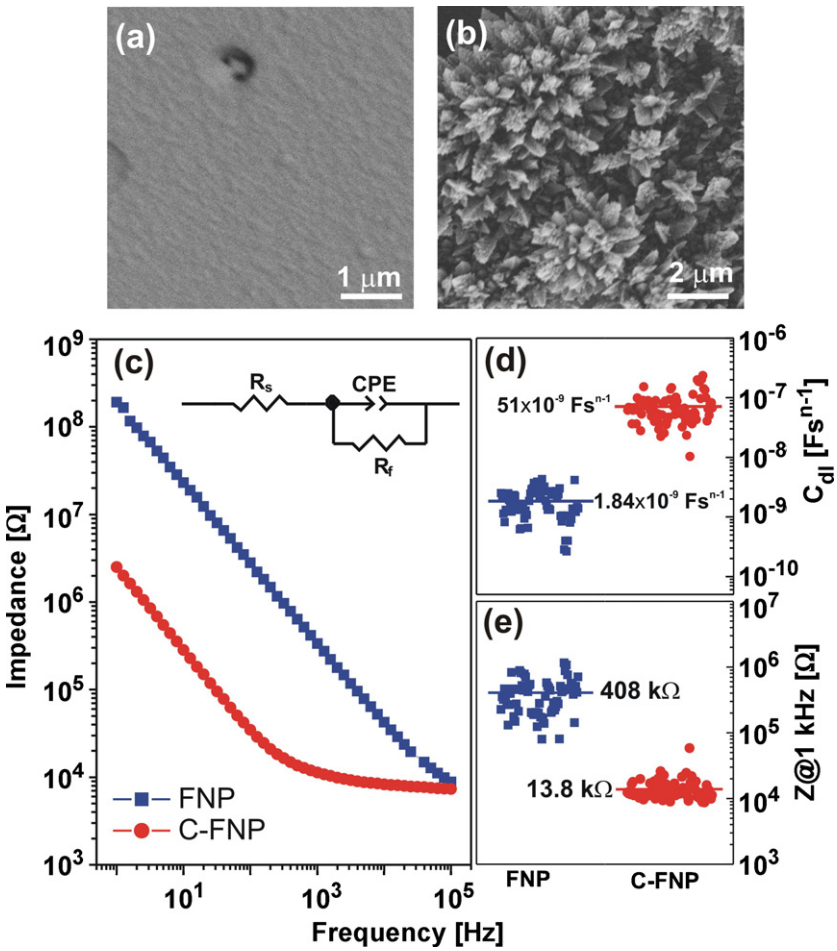

Fig. 6. In vitro results of FNPs. SEM images of the stimulation site of (a) FNP and (b) C-FNP. (c) The EIS spectra of a representative FNP and C-FNP. The insert shows the equivalent circuit model for charge conduction. The extracted values of (d) C_{dl} and (e) interfacial impedance at 1 kHz from EIS ($N = 50$ stimulation sites).

double layer reversibly charges, and then the probe begins to transfer into the Faradaic reactions as the potential moves in a negative direction. The anodic pulse then causes the probe potential to move back in a positive direction. Because not all of the charge injected during the cathodic pulse went into charging of the double layer, the probe potential at the end of the anodic phase is more positive than the pre-pulse potential owning to the unrecoverable charge of the irreversible Faradaic reactions (Merrill et al., 2005).

While the magnitude of the abdominal movements of the moths increased with increasing magnitude of the stimulation signal as shown in Fig. 7a, the direction of the abdominal motion depended on the specific stimulation sites selected. A total of 9 stimulation site pairs were employed for the stimulation experiments across eight moths. These site pairs were either used for monopolar stimulation, where one of the stimulation sites (site 1–5, Fig. 5c) was in contact with the VNC and the second stimulation site (site 6, Fig. 5b) was located at a distance from the VNC (i.e. reference electrode), or for bipolar stimulation where both stimulation sites were adjacent to each other and located on the VNC.

We found that the redesigned FNP could elicit both left ($105^\circ \leq \theta \leq 255^\circ$) and right ($-75^\circ \leq \theta \leq 75^\circ$) abdominal movements from each animal (Fig. 8). Moreover, specific site pairs consistently evoked a given movement (right or left) across all animals. For example, site pairs delivering electrical stimuli to the left hemi-connective of the VNC, i.e. (1, 6), (2, 6) and (1, 2), always (8/8 animals) evoked left abdominal motions (Fig. 8). Alternatively, site pairs delivering electrical stimuli to the right hemi-connective of the VNC, i.e. (4, 6), (5, 6) and (5, 4), almost always (≥7/8 animals) evoked right abdominal motions.

Notably, site pair (3, 6) exhibited poor consistency across the animals. While 4 of the 8 moths gave right abdominal movements, 2 of the 8 moths gave left abdominal movements with stimulation (Fig. 8). Moreover, 2 of 8 moths showed unspecific abdominal movement, for example, a significant change in the direction of the abdominal movements when we increased the magnitude of the stimulation signal (Fig. 8). We believe that this inconsistency occurred because site 3 was placed between the left and right hemi-connectives of the VNC during implantation. Thus, electrical stimuli delivered through site 3 could simultaneously excite axons on both the left and right hemi-connectives depending on exactly where site 3 was positioned during implantation in any given animal. In contrast, site pairs (2, 3) and (4, 3) gave more consistent responses, with 6 of the 8 moths showing left abdominal movements for (2, 3) and 7 of the 8 moths, right abdominal movements for (4, 3). We surmise that this is because biphasic current pulses were employed for the stimulation and current thresholds for excitation with an anodal current typically were 5–8 times larger than the threshold current for direct cathodal stimulation (He, 2005). Therefore the first site (i.e., 2 or 4) would dominate the excitation process over the second site (i.e., 3). Thus, relatively consistent responses were achieved in the site pairs of (2, 3) and (4, 3) in compared to that of site pair (3, 6).

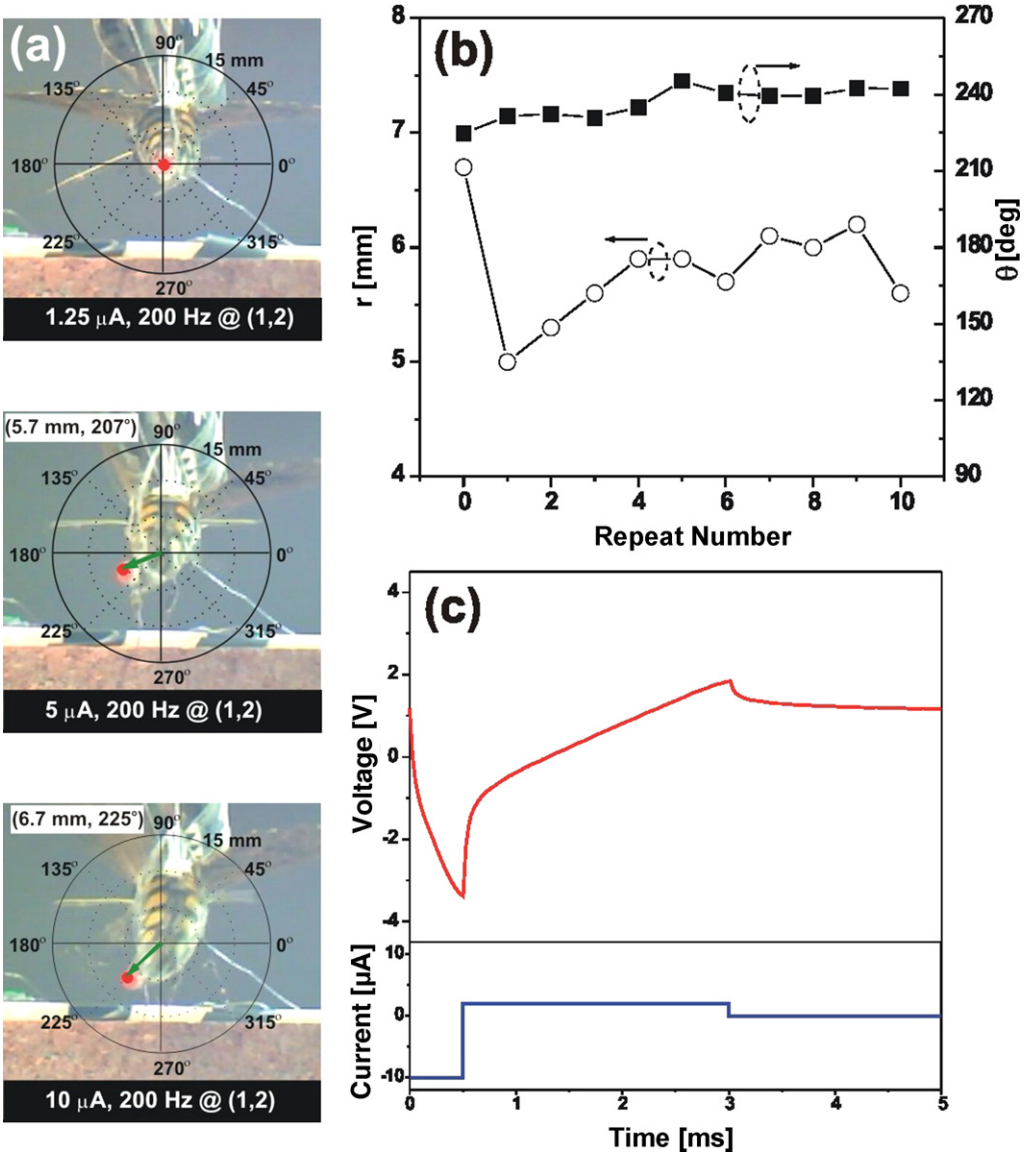

Fig. 7. *In vivo* results of FNPs. (a) Images showing the maximal abdominal movements of a moth following FNP stimulation using site pair (1, 2) at various current strengths indicated in black box at bottom of each image. (b) Variation of the magnitude (r, filled squares) and the direction (θ, open circles) of the abdominal movement with ten successive 10 μA stimulations. (c) Measured voltage waveform across the site pair with the corresponding stimulation current pulse shown below.

We also determined the threshold charge density per phase (Q_{th}/ph) and energy dissipated per cycle (E_{th}/cyc) for eliciting a detectable abdominal movement (>0.5 mm) in the moths for the stimulation pairs (Table 1). We estimated the dissipated energy from the time integration of product of threshold current and its corresponding voltage curve over one cycle of the stimulus, whereas to estimate the charge density we divided the time integration of threshold current over half (one phase) of one cycle of the stimulus by area of the first site of these stimulation pairs, which dominated the excitation process. The Q_{th}/ph is generally adopted in the literature for describing the stimulation ability of the probe. Also, we are interested in energy efficiency of these site pairs for eliciting abdominal movements because portable neural stimulation systems are typically energy constrained.

We observed no noticeable trend in the dissipated energy, which was smallest for electrodes on one side of the FNP (1, 2 with ~3.6–5.9 nJ) and largest for electrodes on the other side (5, 4 with ~5.9–6.6 nJ). The dissipated energy is proportional to the interfacial impedance that critically depends on the electrode implantation in any given animal. Hence, a large fluctuation in the value of E_{th}/cyc is achieved among the animals. For example, the average and standard derivation of E_{th}/cyc for site pair (5, 6) are determined to be 5.9 and 6.4 nJ, respectively, hence, the fluctuation is more than 100%. In

Table 1
Threshold charge per phase (Q_{th}/ph) and energy dissipated per cycle (E_{th}/ph) for evoking an observable abdominal movement on the moth (N = 8 moths).

	Q_{th}/ph (mC/cm^2)	E_{th}/cyc (nJ)
(1,6)	0.17 ± 0.10	3.6 ± 2.2
(5,6)	0.17 ± 0.10	5.9 ± 6.4
(3,6)	0.65 ± 0.11	3.4 ± 2.8
(2,6)	0.44 ± 0.15	5.9 ± 4.8
(4,6)	0.42 ± 0.28	6.6 ± 2.6
(2,1)	0.19 ± 0.09	7.5 ± 6.4
(4,5)	0.21 ± 0.13	8.7 ± 6.8
(3,2)	0.31 ± 0.15	4.5 ± 2.3
(3,4)	0.53 ± 0.32	7.6 ± 6.2

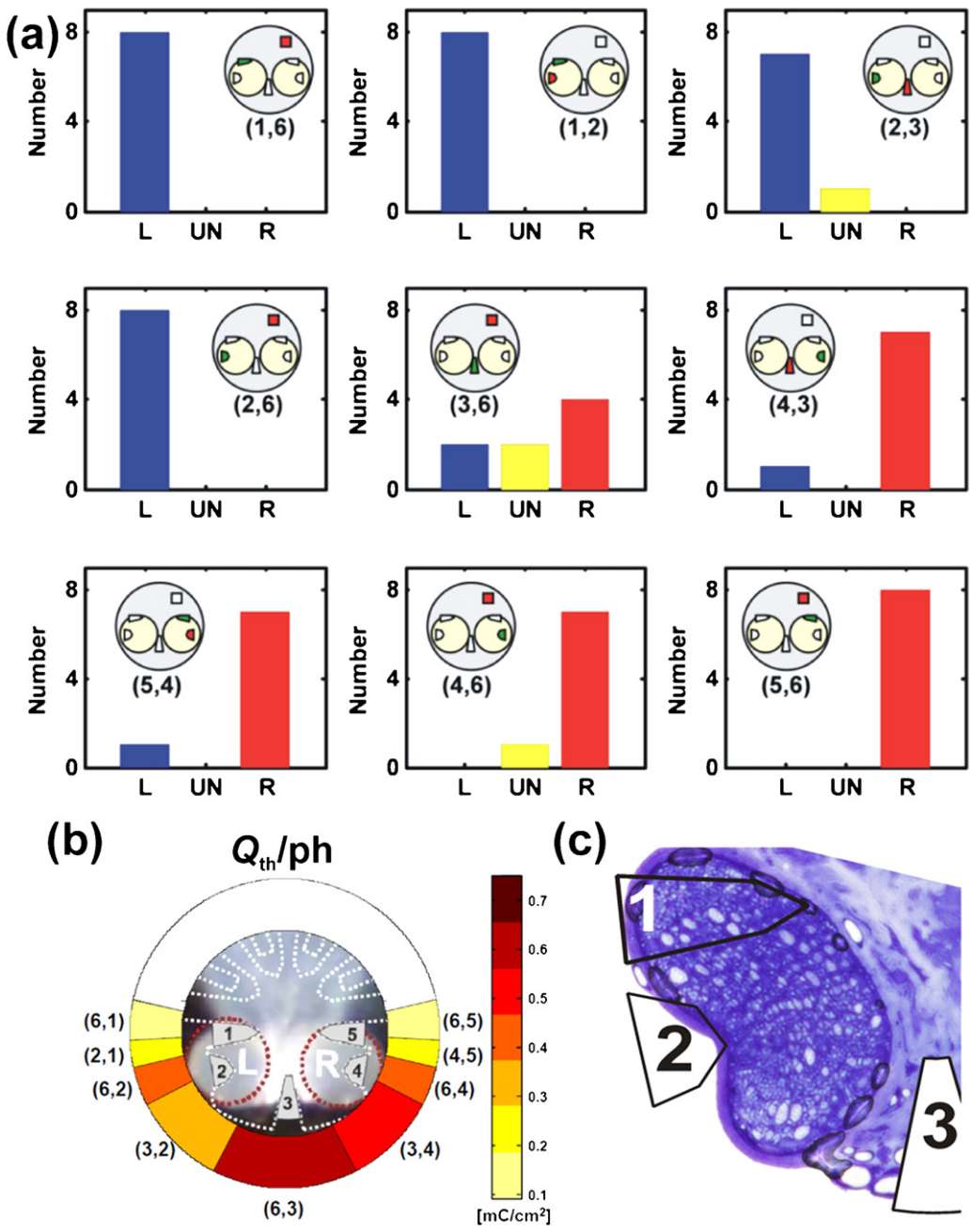

Fig. 8. Statistical results of the moth stimulations from 8 individual animals. (a) Direction of moth abdominal movements following stimulation through various site pairs (indicated in sets). R: right abdominal movement; L: left abdominal movement; UN: unspecific abdominal movement. (b) The spatial distribution of Q_{th}/ph for the various sites pairs with respected to the anatomical structure of VNC, qualitatively. The active regions on the VNC with in response to the stimulations are expected to be around the first site of these site pairs. The active region for the monopolar stimulation is more spread than the bipolar stimulation. (c) Image of a cross section of the left hemi-connective of the adult moth overlaid with scaled schematized drawings of the split-ring of the FNP.

comparison, we observed clear geometrical trends for the threshold charge density as qualitatively shown in Fig. 8b. The threshold charge densities were geometrically symmetric, in that the values for sites 1 and 2 located on the left circle of the split-ring were similar to those of sites 5 and 4 located on the right circle of the split-ring, respectively; site pairs (1,6) and (5,6) both had Q_{th}/ph of 0.17 mC/cm^2 and site pairs (2,6) and (4,6) both had Q_{th}/ph of ~0.42–0.44 mC/cm^2.

Moreover, for both monopolar and bipolar stimulations, site pairs containing either site 1 or 5 had the smallest values of Q_{th}/ph (~0.17 mC/cm^2) while site pairs containing site 3 had the highest threshold charge density (~0.65 mC/cm^2). This is consistent with cross-sectional images of the hemi-connectives (Fig. 8c), which show that the majority of giant axons appear run in the hemi-connectives near where sites 1 (and 5) contact the neural tissue. Because the threshold current for generation of action potentials decreases inversely with the radius of the axon (He, 2005), it is reasonable to expect that electrodes situated near the giant axons would be effective at lower threshold charge densities. The symmetry and the site dependency on the Q_{th}/ph support the idea that the improved FNP was geometrically matched to the anatomical bi-cylindrical structure of the VNC.

In summary, the improved FNP could consistently elicit both left and right abdominal movements in all tested animals. The

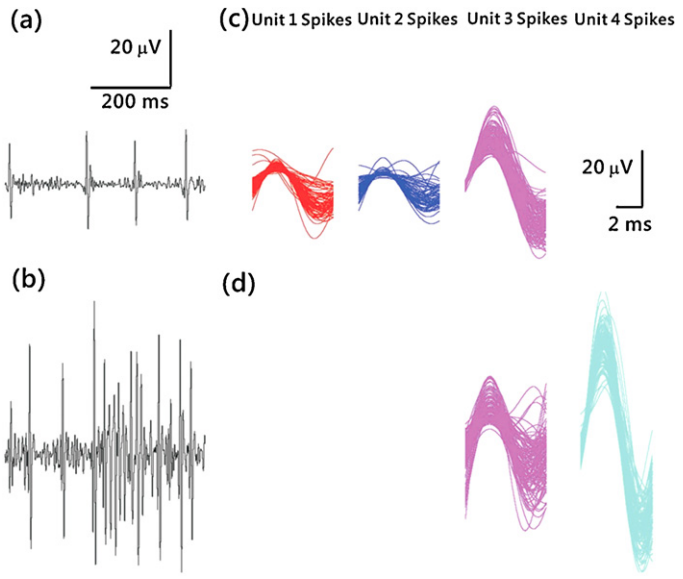

Fig. 9. Multi-unit neural recordings from the VNC of a moth using site pair (2, 6) of the C-FNP. When animal was (a) quiescent and (b) engaged in abdominal movement. Sorted spike waveforms from isolated units from the quiescent state (c) and active state (d) are shown using different colors. Scale bars: vertical = 20 μV, horizontal = 200 ms (a,b); 2 ms (c,d).

direction of the abdominal movements depended on the location on the VNC of the first stimulation site of each site pair, and the magnitude of movement increased with the magnitude of the stimulation signal. Moreover, the threshold charge densities were geometrically symmetric within the bi-circle structure of the split-ring, with stimulation pairs including either site 1 or site 5 having the lowest values of Q_{th}/ph.

3.4. Neural recording

With the improved geometry and addition of the CNT-Au nanocomposite, we sought to demonstrate the ability of the FNPs to record neuronal signals from moths. Given that our stimulation experiments suggested improved local placement of electrodes near axons, and that the CNT-Au nanocomposite resulted in decreased interfacial impedance, we believed that the electrodes would be capable of measuring evoked extracellular potentials. Our demonstration of this capability extends the potential uses of the devices from purely stimulatory to also include recording.

We obtained extracellular recordings from the VNC of moths using the improved FNPs coated with CNT-Au nanocomposite. Multi-unit extracellular activity was recorded when the animal was quiescent (Fig. 9a and c). We attribute this to spontaneous neuronal activity, with regards to abdominal movement. We also recorded extracellular activity when the abdomen was moving (Fig. 9b and d). Under these conditions units fired at higher frequency than in the quiescent condition (unit 3 firing = 4.1 Hz when resting, 22.4 Hz during abdominal motion), and we were able to observe larger spikes that had not been in evidence when the abdomen was at rest (unit 4). Taken together, these experiments demonstrate the ability of the FNPs to record evoked action potentials in behaving animals.

3.5. Wireless flight biasing

Finally, to evaluate the possibility of creating i-MAVs using the CNT-Au nanocomposite-coated FNPs, we attempted to bias the flight of freely flying moths using FNP stimulation through a wireless stimulator (Fig. 1). We found that the improved FNP could evoke multi-directional abdominal movements of the moths using the wireless stimulator (not shown). Importantly, in the flight control experiment, we were able to induce a freely flying animal to perform left and right turning motions using C-FNP stimulation with different site pairs (Fig. 10a, Supplementary Movie 1) based on the fact that abdominal ruddering occurs with these elicited abdominal motions. Moreover, the turning motions were repeatable for successive C-FNP stimulations (Fig. 10b, Supplementary Movie 2).

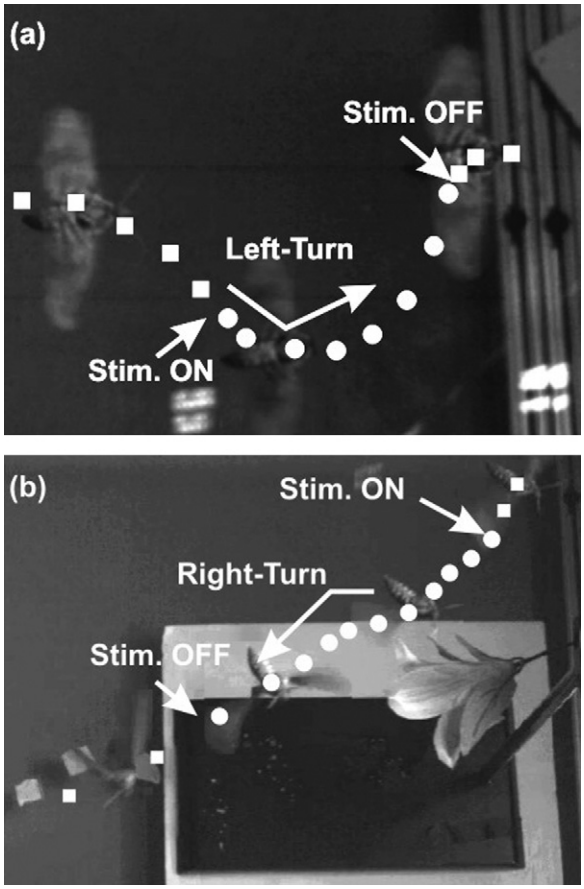

Fig. 10. Images showing a freely flying moth as it performs. (a) Left and (b) right turns following stimulation using C-FNP sites (4, 3) and (1, 3) through a wireless stimulator, respectively. Time points in which the stimulator was off are shown with square markers, while time points during stimulation are indicated with circles.

4. Conclusions

We have developed flexible neural probes (FNPs) that serve as bi-directional insect-machine interfaces with the central nervous system of the moth *Manduca sexta*. The FNPs are not only able to deliver electrical stimuli to the VNC of the moths, evoking multi-directional abdominal movements, but are also able to capture neuronal signals from the VNC of the moths. By improving the geometry of the FNPs to accommodate the anatomical bi-cylindrical structure of insect's VNC, we were able to achieve consistent abdominal movements. Additionally, we have integrated CNT-Au nanocomposites into the FNPs to reduce the interfacial impedance, allowing a decrease in the stimulation voltage. Finally, we demonstrated flight biasing of freely flying moths using C-FNP stimulation with a wireless stimulator.

Acknowledgements

This work was supported by the Air Force Research Laboratory as part of the DARPA HI-MEMS program. We thank the Microsystems Technology Laboratories for fabrication assistance. We thank Spencer Murray and Sam Sinai for assistance with FNP implantation, characterization and stimulation. We would also like to acknowledge, Margaret Marez, and Binh Nyugen for care and rearing of moths.

Appendix A. Supplementary data

Supplementary data associated with this article can be found, in the online version, at doi:10.1016/j.jneumeth.2011.11.026.

References

Bozkurt A, Gilmour RF, Lal A. Balloon-assisted flight of radio-controlled insect biobots. IEEE Transactions on Biomedical Engineering 2009;56:2304–7.

Burrows M. The neurobiology of an insect brain. Oxford University Press; 1996.

Daly DC, Mercier PP, Bhardwaj M, Stone AL, Aldworth ZN, Daniel TL, et al. A pulsed UWB receiver SoC for insect motion control. IEEE Journal of Solid-State Circuits 2010;45:153–66.

Gray JR, Pawlowski V, Willis MA. A method for recording behavior and multineuronal CNS activity from tethered insects flying in virtual space. Journal of Neuroscience Methods 2002;120:211–23.

Harrison RR, Fotowat H, Chan R, Kier RJ, Leonardo A, Gabbiani F. A wireless neural/EMG telemetry system for freely moving insects. In: Proceedings of the 2010 IEEE International Symposium on Circuits and Systems; 2010. p. 2940–3.

He B. (editor). Neural Engineering. Kluwer Academic/Plenum Publishers, 2005.

Keefer EW, Botterman BR, Romero MI, Rossi AF, Gross GW. Carbon nanotube coating improves neuronal recordings. Nature Nanotechnology 2008;3:434–9.

Lemmerhirt DR, Staudacher EM, Wise KD. A multitransducer microsystem for insect monitoring and control. IEEE Transactions on Biomedical Engineering 2006;53:2084–91.

Lovat V, Pantarotto D, Lagostena L, Cacciari B, Grandolfo M, Righi M, et al. Carbon nanotube substrates boost neuronal electrical signaling. Nano Letters 2005;5:1107–10.

Malleo D, Nevill JT, van Ooyen A, Schnakenberg U, Lee LP, Morgan H. Note characterization of electrode materials for dielectric spectroscopy. Review of Scientific Instruments 2010:81.

Merrill DR, Bikson M, Jefferys JGR. Electrical stimulation of excitable tissue: design of efficacious and safe protocols. Journal of Neuroscience Methods 2005;141:171–98.

Peckham PH, Knutson JS. Functional electrical stimulation for neuromuscular applications. Annual Review of Biomedical Engineering 2005;7:327–60.

Quiroga RQ, Nadasdy Z, Ben-Shaul Y. Unsupervised spike detection and sorting with wavelets and superparamagnetic clustering. Neural Computation 2004;16:1661–87.

Sato H, Berry CW, Peeri Y, Brendan EB, Casey BE, Lavella G, et al. Remote radio control of insect flight. Frontiers in Integrative Neuroscience 2009;3:1–11.

Spence AJ, Neeves KB, Murphy D, Sponberg S, Land BR, Hoy RR, et al. Flexible multielectrodes can resolve multiple muscles in an insect appendage. Journal of Neuroscience Methods 2007;159:116–24.

Takeuchi S, Shimoyama I. A three-dimensional shape memory alloy microelectrode with clipping structure for insect neural recording. Journal of Microelectromechanical Systems 2000;9:24–31.

Tsang WM, Stone AL, Aldworth ZN, Hildebrand JG, Daniel TL, Akinwande AI, et al. Flexible split-ring electrode for insect flight biasing using multisite neural stimulation. IEEE Transactions on Biomedical Engineering 2010;57:1757–64.

Voge CM, Stegemann JP. Carbon nanotubes in neural interfacing applications. Journal of Neural Engineering 2011:8.

Ye S, Dowd JP, Comer CM. A motion tracking system for simultaneous recording of rapid locomotion and neural activity from an insect. Journal of Neuroscience Methods 1995;60:199–210.